Electronic Supplementary Information

Reversible K-Ion Intercalation in $CrSe_2$ Cathodes for Potassium-Ion Batteries: Combined Operando PXRD and DFT studies

Weihao Li,[a] Johannes Döhn,[b] Jinyu Chen,[cd] Manuel Dillenz,[b] Mohsen Sotoudeh,[b] David M. Pickup,[e] Shunrui Luo,[f] Ryan Parmenter,[e] Jordi Arbiol,[fg] Maria Alfredsson,[e] Alan V. Chadwick,[e] Axel Groβ,[bh] Maider Zarrabeitia *[cd] and Alexey Y. Ganin *[a]

a. School of Chemistry, University of Glasgow, G12 8QQ, Glasgow, United Kingdom. Email: Alexey.Ganin@glasgow.ac.uk

b. Institute of Theoretical Chemistry, Ulm University, 89081, Ulm, Germany

c. Helmholtz Institute Ulm (HIU) Helmholtzstrasse 11, 89081, Ulm, Germany. Email: maider.ipina@kit.edu

d. Karlsruhe Institute of Technology (KIT), P.O. Box 3640, D-76021 Karlsruhe, Germany

e. School of Physical Sciences, University of Kent, CT2 7NH, Canterbury, Kent, United Kingdom

f. Catalan Institute of Nanoscience and Nanotechnology (ICN2), CSIC and BIST, Campus UAB, Bellaterra, 08193 Barcelona, Catalonia, Spain

g. ICREA, Pg. Lluís Companys 23, 08010 Barcelona, Catalonia, Spain

h. Helmholtz Institute Ulm (HIU) for Electrochemical Energy Storage, 89081, Ulm, Germany.

Supplementary Note 1

Material preparation

Synthesis of pristine $KCrSe_2$ was carried out on a 400 mg scale the reagents and products of reaction handled inside an argon-filled glove box (MBraun, <0.1 ppm of O_2). Stoichiometric amounts of Cr powder (Alfa Aesar, 99.94%, -200 mesh, metal basis), Se shots (Alfa Aesar, 99.99%, metal basis) and graphite powder (Fisher Scientific, -100 mesh, 99.9995 %, metal basis) were loaded into a Pyrex insert together with K metal (Fisher Scientific, 99.9%, metal basis). The insert was placed inside a Pyrex ampoule and sealed under vacuum with a blow torch. The ampoule was then placed upright in a muffle box furnace and heated at 250°C (1°C min^{-1} ramp) for 4 hours. The temperature was then raised to 600°C (1°C min^{-1} heating ramp, 72 h dwell, 5°C min^{-1} cooling). The sample was then taken out of the ampoule, ground using mortar and pestle, sealed under vacuum again and further reannealed at 600°C (1°C min^{-1} heating ramp, 48 h dwell, 5°C min^{-1} cooling ramp). Synthesis of $KCrSe_2$ with addition 10 wt. % of graphite was carried out on the same scale and under identical synthetic protocol.

Pristine $CrSe_2$ was prepared by the deintercalation of pristine $KCrSe_2$ powders with iodine in acetonitrile solution respectively. Inside an argon-filled glove box (MBraun, <0.1 ppm of O_2), 200 mg of $KCrSe_2$ powder was loaded into a round bottom flask equipped with a stirring bar. The flask was attached to a Schlenk line and *ca*. 4 mL (given in excess) of 0.5 M iodine in acetonitrile solution (Fisher Scientific, anhydrous, 99.8 %) was added under N_2 flow. The mixture was stirred 24 hours at ambient temperature (~20°C). The product was then filtered in air, resulting in a black powder on the filter. The powder was washed with 100 ml of acetonitrile, then with excess of deionised water, finally rinsed with 100 ml of ethanol and left to dry overnight in an evacuated desiccator. The synthesis of $CrSe_2$ with 10 wt. % of graphite were carried out on the same scale from $KCrSe_2$ with addition 10 wt. % of graphite by using identical synthetic protocol.

Electrolyte

Potassium hexafluorophosphate (KPF_6,≥99%, Sigma Aldrich), ethylene carbonate (EC, battery grade, UBE), dimethyl carbonate (DMC, battery grade, UBE), N-methyl pyrrolidone (NMP, anhydrous, Sigma Aldrich), K metal (98 %, in mineral, Sigma Aldrich), polyvinylidene fluoride (PVDF, Solef 6020, Solvay) and carbon black (Super C65, Imerys).

Electrochemical characterization

The Graphite-added $CrSe_2$ active material was mixed with PVDF binder and Super C_{65} conductive carbon in a weight ratio of 80:10:10 and dissolved in NMP. The slurry was cast onto aluminum foil (battery grade) and dried at 80 °C overnight in an oven. The resulting electrode sheet was punched with a diameter of 12 mm and further dried in a Büchi oven at 80 °C for 24 hours under vacuum. Subsequently, the electrodes were pressed at 4000 kg cm^{-2} for 30 s and dried again in a Büchi oven at 80 °C for 2 hours under vacuum before cell assembly. The electrodes were directly transferred in a sealed vessel and stored in an ultrapure Argon-filled glovebox (MBraun, H_2O, and O_2 content < 0.1 ppm) for cell assembly. The active material mass loading was about 2.5 ± 0.1 mg cm^{-2}, with a 69.5 wt% of $CrSe_2$ active materials. The 12 mm K metal disks were prepared following the reported work.[1] The K metal was soaked in an excess of electrolyte solution (1M KPF_6 EC/DMC (1:1, V/V)), taken out, rolled, obtaining a thin film, and finally punched out.

The cycling performance and rate capability performance were tested in CR2032 coin-cells, using the 12 mm diameter $CrSe_2$ electrode as working electrode, 12 mm diameter K metal as counter and reference electrode, Whatman glass microfiber filters (GF/D) as separator and 1M KPF_6 EC/DMC (1:1, V/V) (100 µL) as electrolyte. After a rest time of 6 hours, the galvanostatic cycling or rate capability tests were performed within a voltage range spanning from 1.0 V to 3.5 V vs. K^+/K by using a Maccor 4000 battery tester. The galvanostatic cycles were tested applying a constant current of 12.7 mA g^{-1} (≈1/10C, nominal capacity is 127 mAh g^{-1}, corresponding to $CrSe_2$ theoretical capacity), and the C-rate measurement from 0.1C to 1 C. All electrochemical measurements were performed in climatic chambers (Binder GmbH) at 20 °C ± 2 °C, if not stated otherwise. The graphite only active material was mixed with PVDF binder and Super C65 conductive carbon in a weight ratio of 80:10:10 and dissolved in NMP. The slurry was cast onto aluminum foil (battery grade) and dried at 80 °C overnight in an oven. The assembly and testing protocol was identical to the one on carried out $CrSe_2$ cathode.

Material characterization

PXRD of non-air-sensitive samples were measured on a Rigaku MiniFlex 6G diffractometer ($CuK_{\alpha1}$ and $CuK_{\alpha2}$ wavelengths - 1.5406 and 1.5444 Å, respectively) equipped with a D/teX Ultra detector operating in the Bragg–Brentano geometry. Powder samples were carefully packed onto zero background holders and levelled using a glass microscope slide. SC electrodes were also tested by attaching them directly to the holder with a double-sided tape.

Diffraction patterns were collected with a step size of 0.015° and time per step of 1° min^{-1}. The sample holder was spined during the measurements at 10 rpm.

PXRD measurements of air-sensitive $KCrSe_2$ samples were performed on a PANalytical Empyrean diffractometer ($CuK_{\alpha1}$ and $CuK_{\alpha2}$ wavelengths - 1.5406 and 1.5444 Å respectively) operating in the Debye-Scherrer geometry. The samples were packed inside an Ar-filled glove box (MBraun, <0.1 ppm O_2) into 0.5 mm diameter (0.1 mm wall thickness) No.50 special glass capillaries (Hilgenberg), which were sealed with a blow torch. The PXRD patterns were collected with a step size of 0.016° and time per step of 5° min^{-1}. To enable a proper comparison with simulated diffraction patterns the background was subtracted in the Highscore Plus Software (Panalytical).

Le Bail refinement of selected PXRD data was performed using GSAS-II software.[2] The refined parameters included unit cell parameters, sample displacement, strain, and crystallite broadening. Background was fitted using shifted Chebyshev polynomic shape.

In-operando PXRD measurements together with GCD data collection using a single-channel potentiostat/galvanostat (SP-200, BioLogic) were performed on Bruker D8 Advance diffractometer with CuK_α radiation (λ=1.5406 nm). The step size of 0.03° and an overall time of about 30 min per scan. A custom-made *in-operando cell* (as described in detail elsewhere [3]) was assembled in an ultrapure Argon-filled glovebox (MBraun, H_2O, and O_2 content < 0.1 ppm) as follows. First, active material with mass loading of about 2.5 ± 0.1 mg cm^{-2} (69.5 wt% of $CrSe_2$ active materials) was deposited on a beryllium window (250 µm, Materion Brush) to serve as the working electrode. 1M KPF6 EC/DMC (1:1, V/V) as electrolyte and a 12 mm diameter piece of K metal was used as the counter electrode, following the same procedure as described earlier. The coated beryllium disc was dried for 2 hours at room temperature and 80 °C in an oven overnight, then it was finally dried in a high-vacuum Büchi oven at 80 °C for 20 hours. The PXRD data were collected in the voltage window of 1.0-3.5 V vs. K^+/K.

Scanning electron microscope/Energy Dispersive X-Ray (SEM / EDX) studies were carried out on small amounts of powders loaded on a sticky carbon tape followed by was shaking it to remove the excess powder. Morphology studies were carried out on a Scanning Electron Microscope (TESCAN CLARA) equipped with a Field Emission Gun electron source which was coupled with an Oxford Instruments UltimMax 65 with an Aztec live interface EDX system for elemental analysis.

Highresolution TEM (HRTEM) analysis images were obtained using a field emission gun FEI™ Tecnai F20 microscope at 200 kV. High angle annular darkfield scanning transmission electron microscope (HAADF-STEM) was combined with an energy-dispersive X-ray spectroscopy (EDX) detector at 15 kV to analyze composition.

Cr and Se K-edge X-ray absorption spectroscopy (XAS) data were collected at beamline B18 at the Diamond Light Source, U.K. Samples were diluted with crystalline cellulose and pressed into a 13 mm diameter pellets using a hydraulic press. Incident X-ray wavelengths were selected using a Si(111) double-crystal monochromator. Extended X-ray absorption fine structure (EXAFS) spectra and X-ray absorption near-edge structure (XANES) spectra were collected in transmission mode using two gas-filled ionization chambers. In the case of the Cr K-edge measurements, a Cr metal foil was placed in front of a third ionization chamber to correct for instrumental drift. For the Se K-edge measurements, a Se foil was not available; instead a Pt metal foil was used since the Pt L2-edge energy of 13.2726 keV is close to the Se K-edge energy of 12.6578 keV. Initial processing of the data, normalization and background removal, was performed using the program ATHENA.[4] The k3-weighted EXAFS spectra were modelled using the program ARTEMIS to determine interatomic Cr-Se, Cr-Cr and Se-Se distances within each sample.

Calculation of the apparent diffusion coefficients

In the intercalation type electrode, the peak current (I_p) has a linear relationship with the square root of scan rate ($v^{1/2}$).[5]

The diffusion coefficient then can be calculated using Randles–Sevcik equation[6]:

$$I_p = (2.69 \times 10^5)\, n^{3/2} A D^{1/2} C v^{1/2} \qquad \text{(Eq. 1)}$$

where I_p is the peak current (A), n is the charge-transfer number of 1, A is the contact area of 1.13 cm^2, C is the concentration of K-ions in the cathode, and v is the potential scan rate (V/s). The peak current I_p against the potential scan rate $v^{1/2}$ gives a straight line (Fig. S9).

The eq. 1 is then can be expressed as follows:

$$Slope = 2.69 \times 10^5\, n^{3/2} A D^{1/2} \qquad \text{(Eq. 2)}$$

From this equation the relevant apparent diffusion coefficient was calculated as $D_{C1} = 7.3 \times 10^{-11}$ cm^2/s (for the deintercalation from Stage 3 to Stage 2) and $D_{C2} = 3.8 \times 10^{-11}$ cm^2/s (for the deintercalation from Stage 2 to Stage 1).

DFT

$CrSe_2$ and $KCrSe_2$ are known to crystalize in space groups *P*-3*m*1 and *C*2/*m* with 3 and 8 atoms in the unit cell,[7] respectively. A DFT benchmark on the structural parameters was performed for both unit cells including the widely used exchange-correlation functional suggested by Perdew, Burke, and Ernzerhof (PBE),[8] its optimized version for solids (PBEsol),[9] and the strongly constrained and appropriately normed (SCAN) meta-generalized gradient

approximation.[10] All functionals sufficiently reproduce the experimentally obtained lattice constants for $KCrSe_2$ except PBEsol which slightly underestimates the *c*-parameter. In the case of $CrSe_2$ all functionals slightly overestimate the lattice constant *a*, the *c*-parameter is only reproduced by PBE and slightly underestimated by SCAN. The PBEsol prediction is far off the experimental value in the latter case.

Additionally, empirical Van-der-Waals corrections were tested for all functionals.[11-13] It is remarkable that in contrast to other layered materials where van-der-Waals interactions are crucial for the description of the layer spacing,[14] in the case of $CrSe_2$ the inclusion of van-der-Waal corrections make the outcomes less reliable.

According to the previous discussion, the PBE functional was used for most of the geometry optimizations and the more computationally expensive SCAN functional was used for certain samples only. The density of states was determined by employing the hybrid HSE06 functional.[15] The ionic cores were treated with the projector augmented wave method,[16] as implemented in the Vienna Ab Initio Simulation Package.[17-19] Electronic wave functions were expanded up to energies of 600 eV and it was made sure that total energies converged within a few meV/atom concerning the number of k-points in the first Brillouin zone. Spin polarized calculations with ferromagnetic initialization were performed throughout the study. All structures were optimized until the entries of the stress tensor and all forces were below 0.01 eV/Å without constraining any internal degree of freedom.

The use of the formation energy E_f to determine the convex hull of stability is common practice[20-22] and has been thoroughly discussed in recent reviews.[23, 24] However, due imperfections of DFT and the negligence of kinetic effects, values above the convex hull may still correspond to (meta-)stable materials and materials on the convex hull may decompose. Consequently, a compelling prediction of a materials' stability is clearly not possible. The estimation of the reliability of such results is a challenging task. In general, assuming the methodological inaccuracy of formation energies of up to 200 meV/atom for PBE calculations is commonly accepted,[25-27] although this number may be significantly reduced in the present analysis due to the chemical similarity of the compared systems. Furthermore, the SCAN functional has been shown to half the error in formation energies leading to significantly improved results.[27]

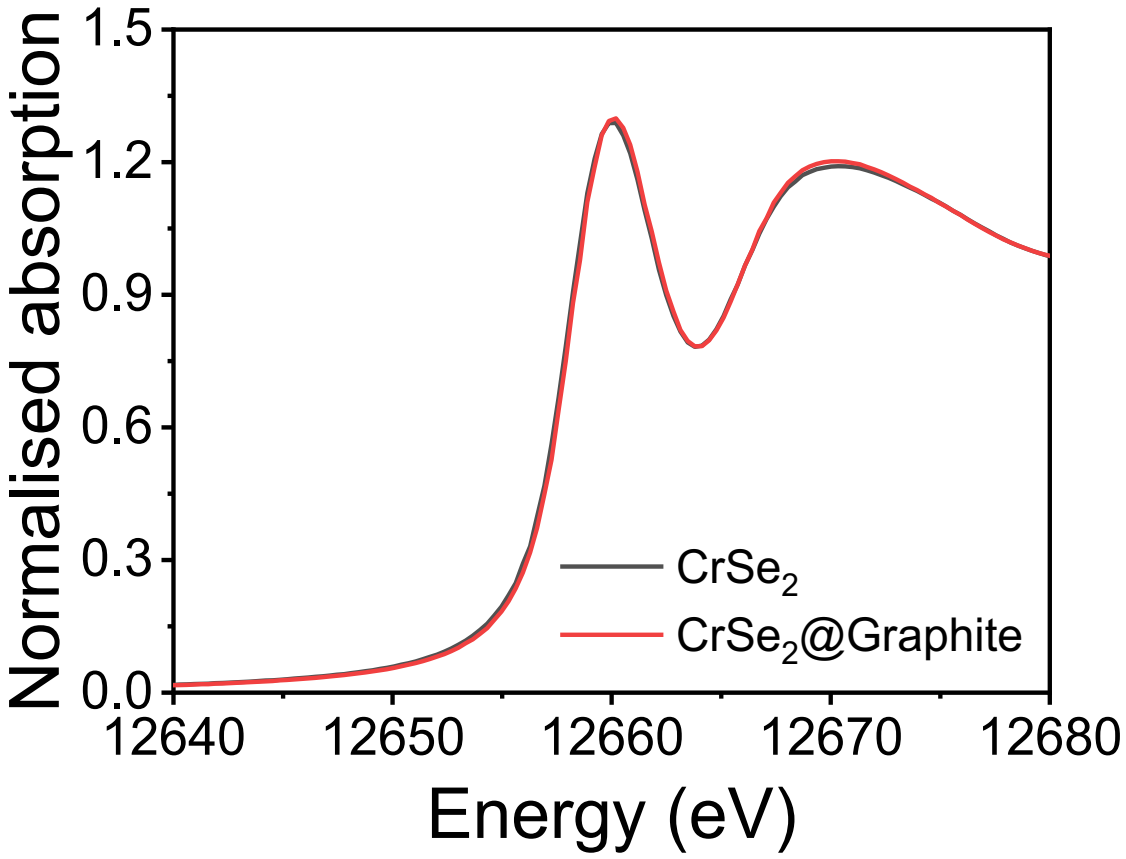

Figure S1. Se K-edge XANES profile of $CrSe_2$ (black) and $CrSe_2$ with an optimal addition of 10 wt. % of graphite (red).

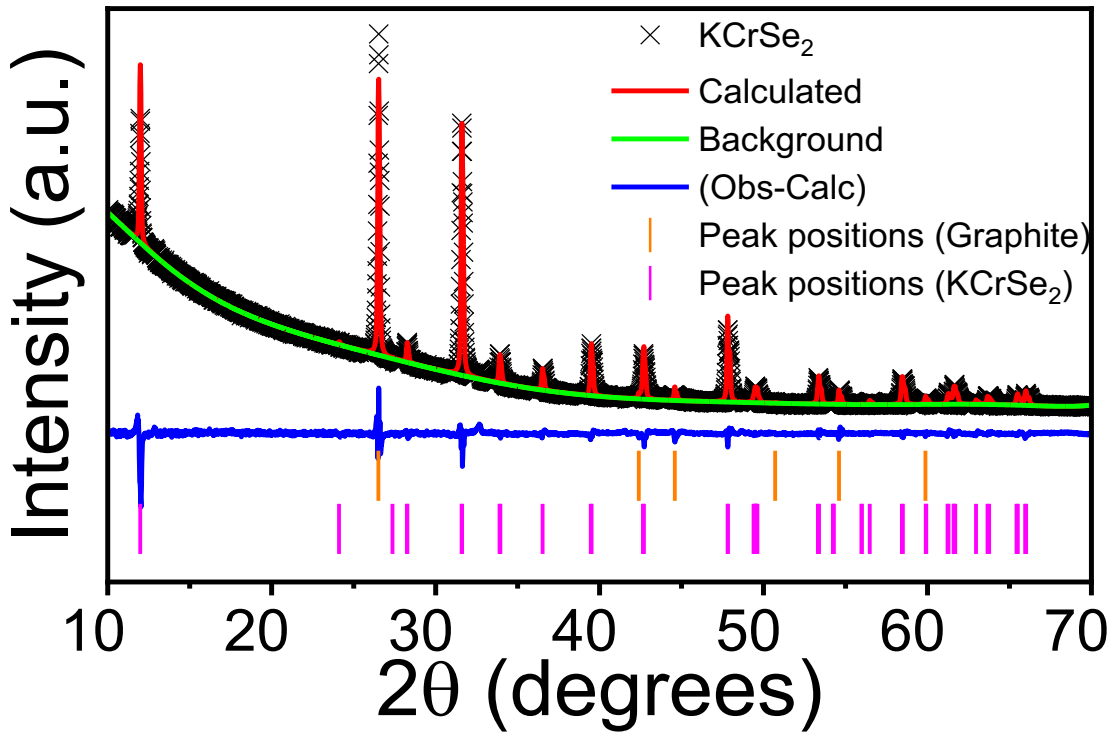

Figure S2. LeBail refinement of the experimental PXRD profile (CuK_{α}) for a sample $KCrSe_2$ with 10 wt. % graphite against a structure model for $KCrSe_2$ and graphite. Measured data are shown as black crosses; the calculated profile is shown by a solid red line. The difference between the calculated and experimental data is shown as a blue profile. Magenta and orange vertical bars represent the reflection positions for the $CrSe_2$ and graphite phases respectively.

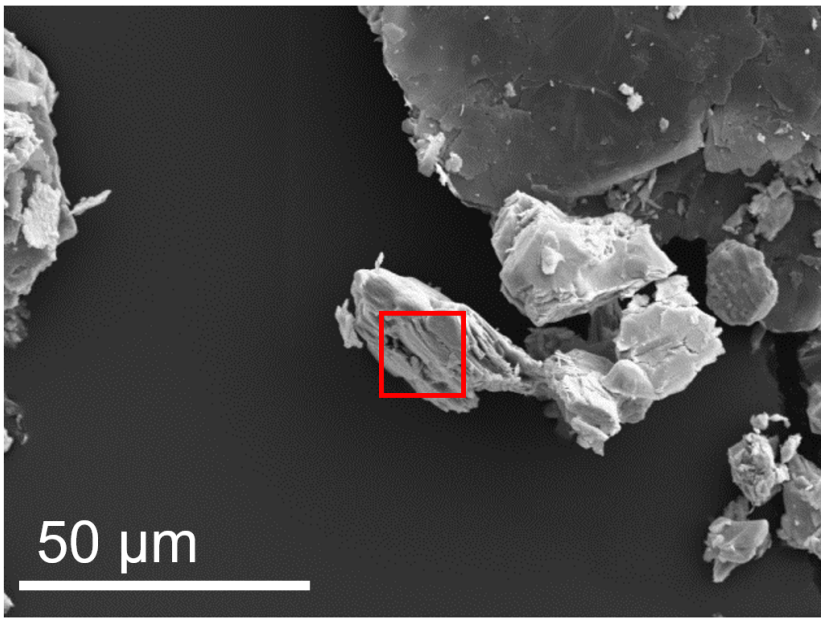

Figure S3. SEM images of $CrSe_2$ with an optimal addition of 10 wt. % of graphite. The red box shows the zoomed in region presented in Fig. 2c.

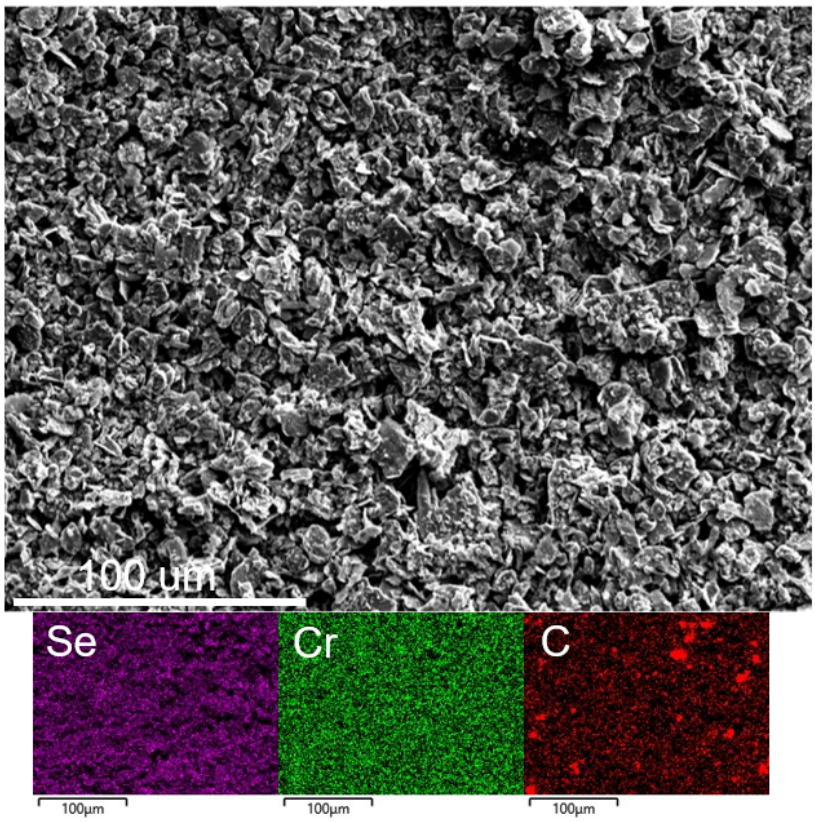

Figure S4. Low resolution SEM images of $CrSe_2$ with an optimal addition of 10 wt. % of graphite and the interposition of the relevant EDX maps for Cr, Se and C on the SEM image.

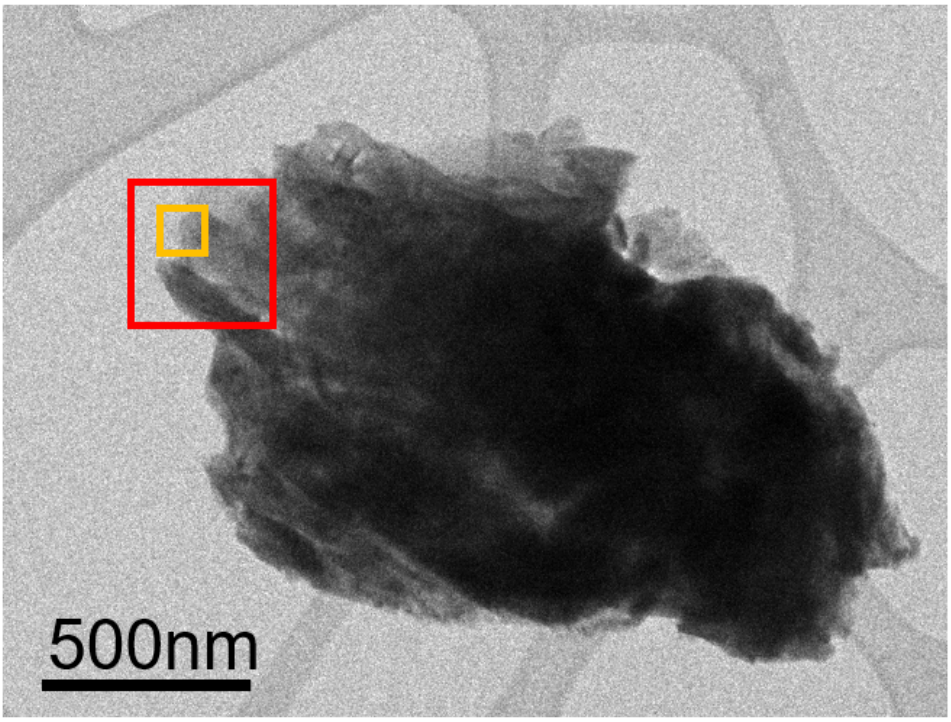

Figure S5. TEM image of $CrSe_2$ with an optimal addition of 10 wt. % of graphite. The orange box is the respective zoomed in areas in Fig. 2d.

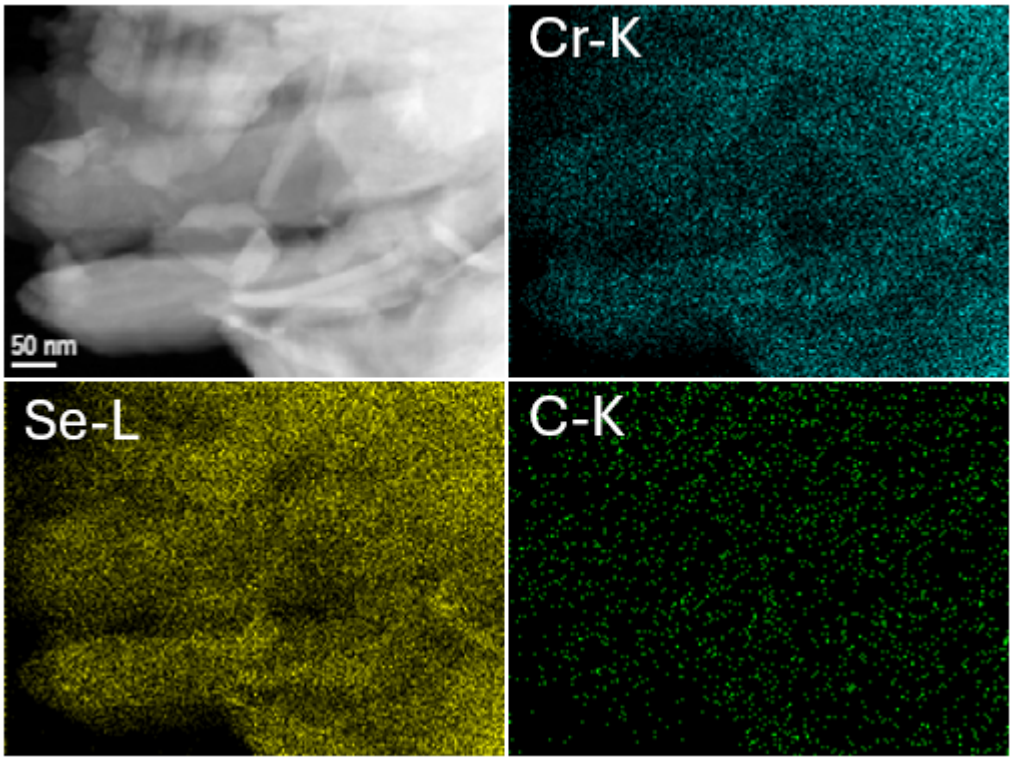

Figure S6. The EDX elemental mapping from the red box region in Fig. S5.

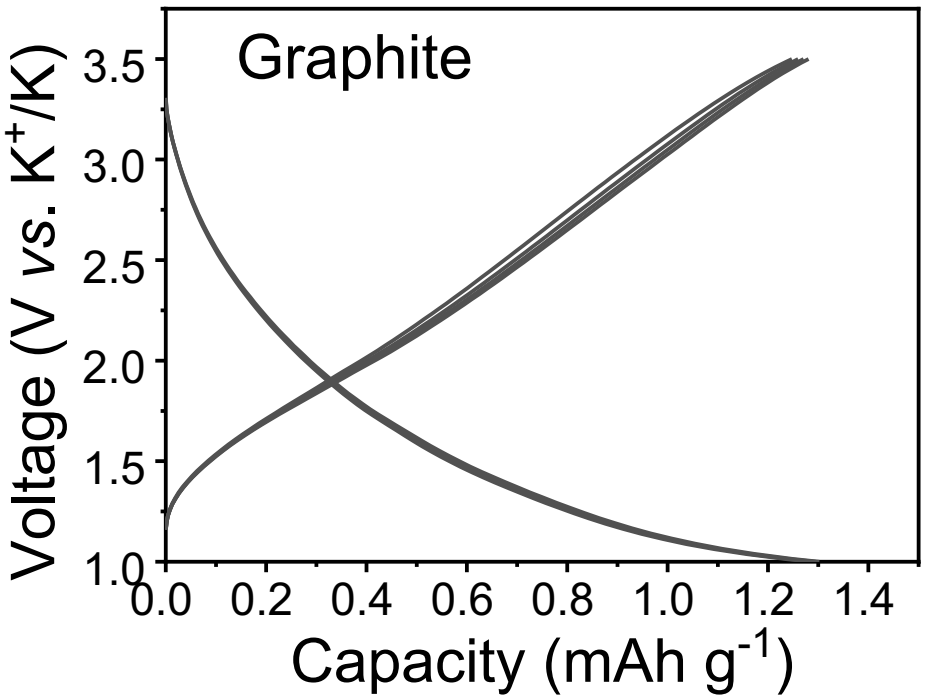

Figure S7. GCD profiles of $CrSe_2$ recorded at 0.1 C scan rate at 20 ºC ± 2 ºC

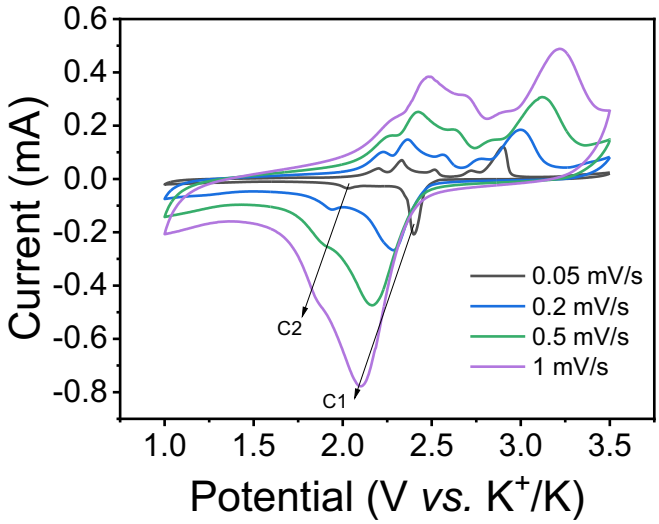

Figure S8. CV curves of $CrSe_2$ at scan rates from the 0.05 mV/s to 1 mV/s.

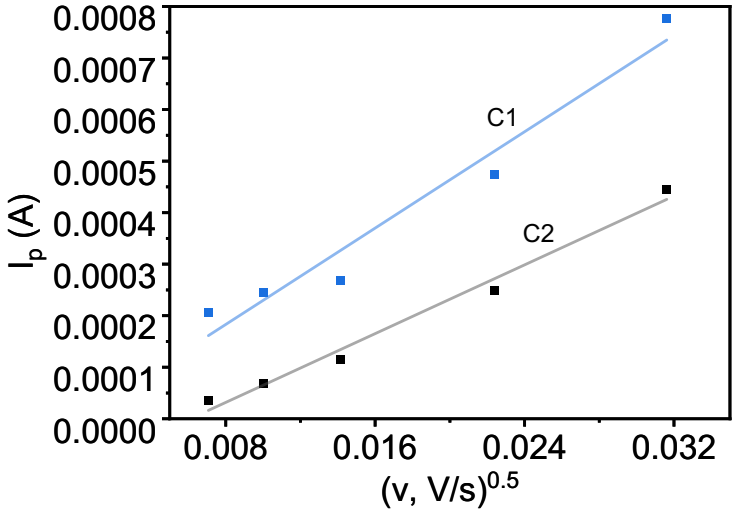

Figure S9. The relationship of the peak current (I_p) and the square root of scan rate ($v^{1/2}$).

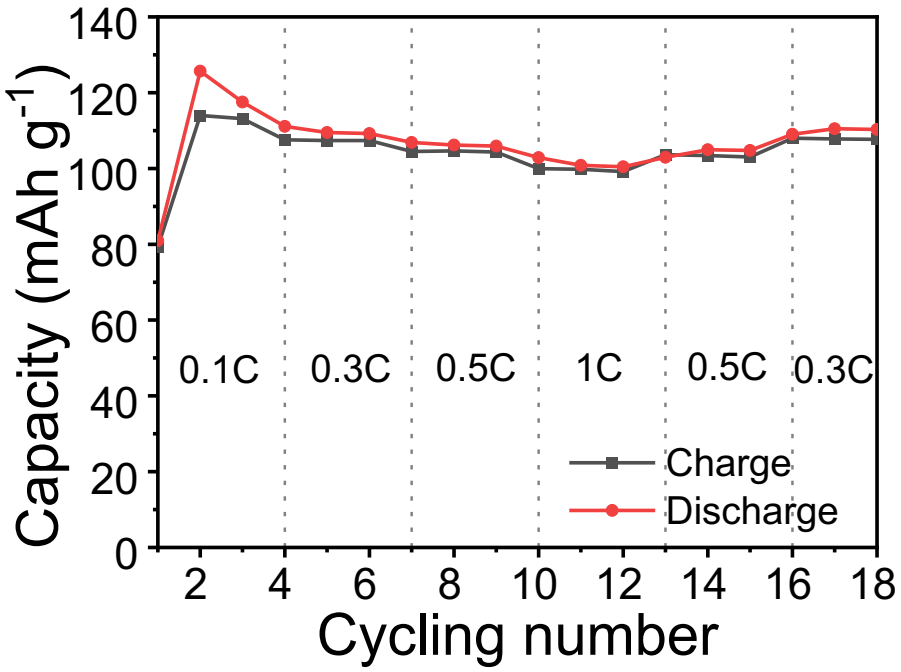

Figure S10. Rate performance and capacity retention of of KIB based on $CrSe_2$ cathode during galvanostatic discharge/charge experiment. The initial 18 cycles (3 cycles each) were carried out at 0.1C, 0.3C, 0.5C, 1C, 0.5C, and 0.3C.

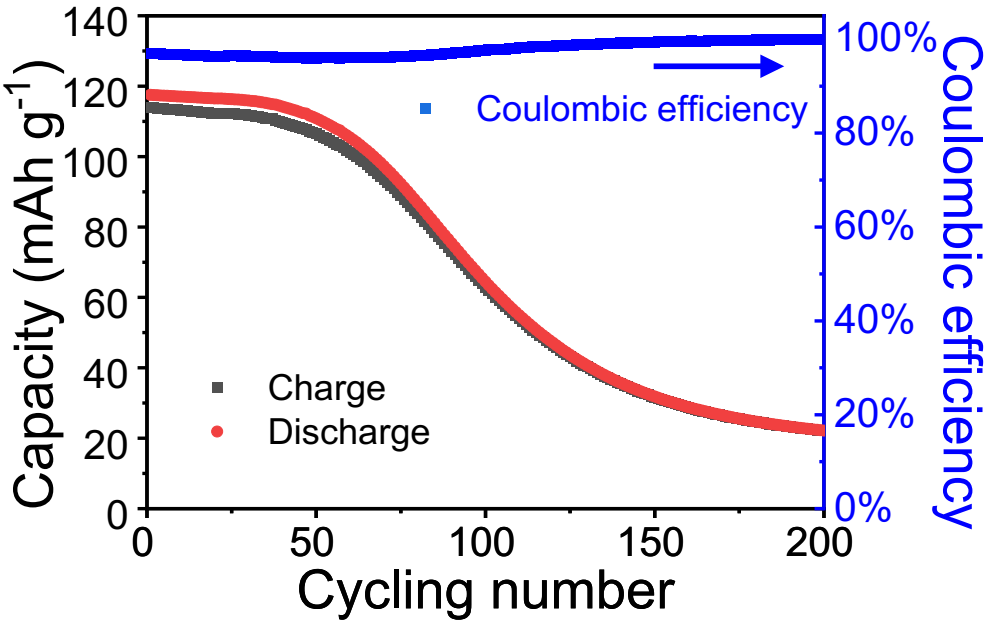

Figure S11. Capacity retention and Coulombic efficiency of a KIB based on $CrSe_2$ cathode during galvanostatic discharge/charge experiment.

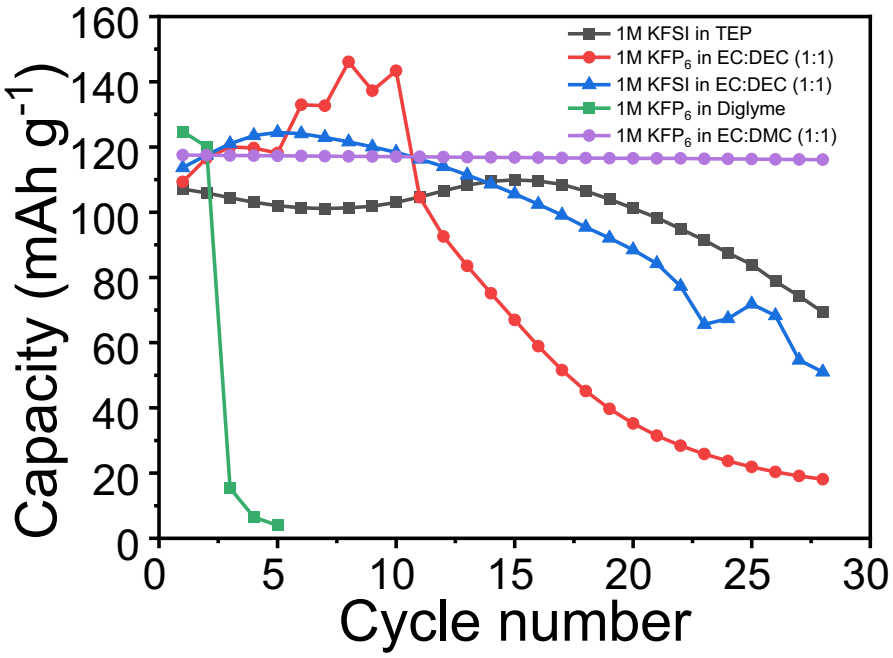

Figure S12. Cycling performance and capacity retention of KIB based on $CrSe_2$ cathode during galvanostatic discharge/charge experiment depending on the nature of the electrolyte.

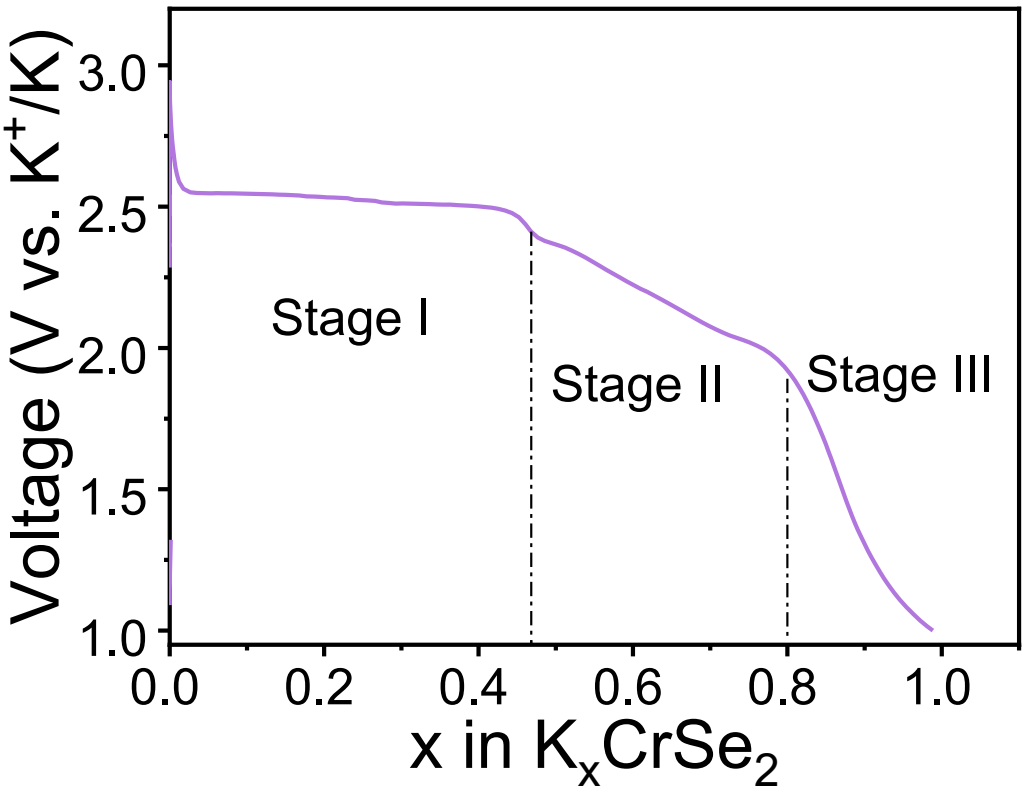

Figure S13. The data from the Figure 3c corresponding to GCD profiles replotted as a value of *x* in K_xCrSe_2. The stage corresponds to a specific phase.

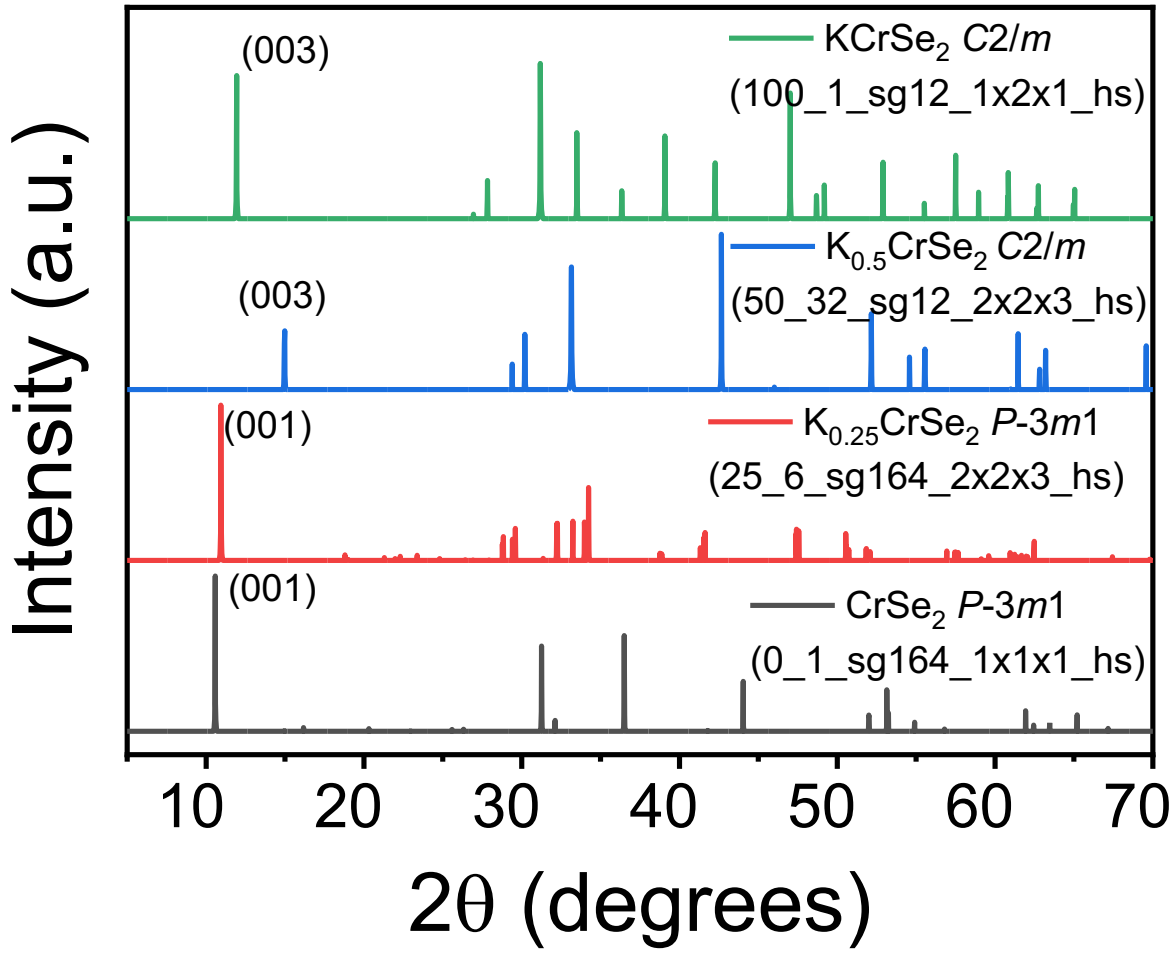

Figure S14. Simulated PXRD patterns of the most energetically stable structures of K_xCrSe_2 based on PBE functional.

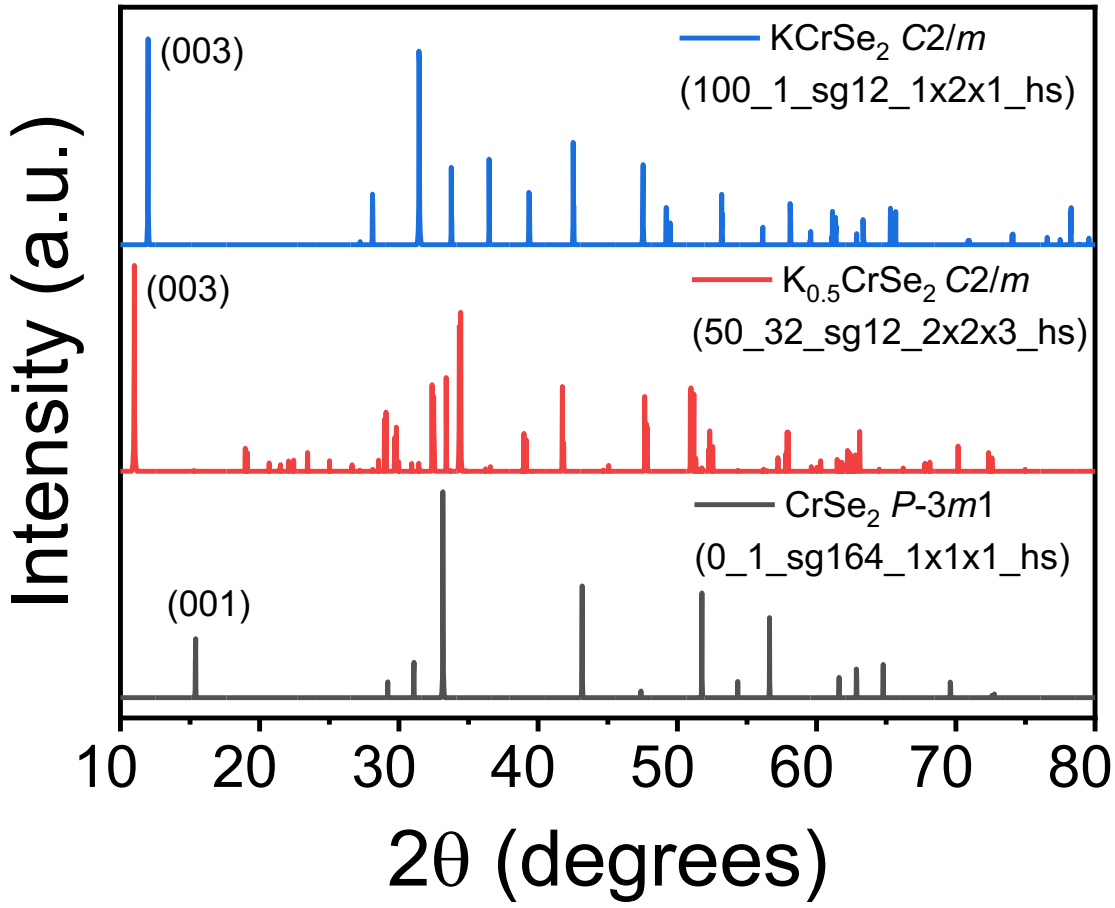

Figure S15. Simulated PXRD patterns of energic stable structures of K_xCrSe_2 based on SCAN functional.

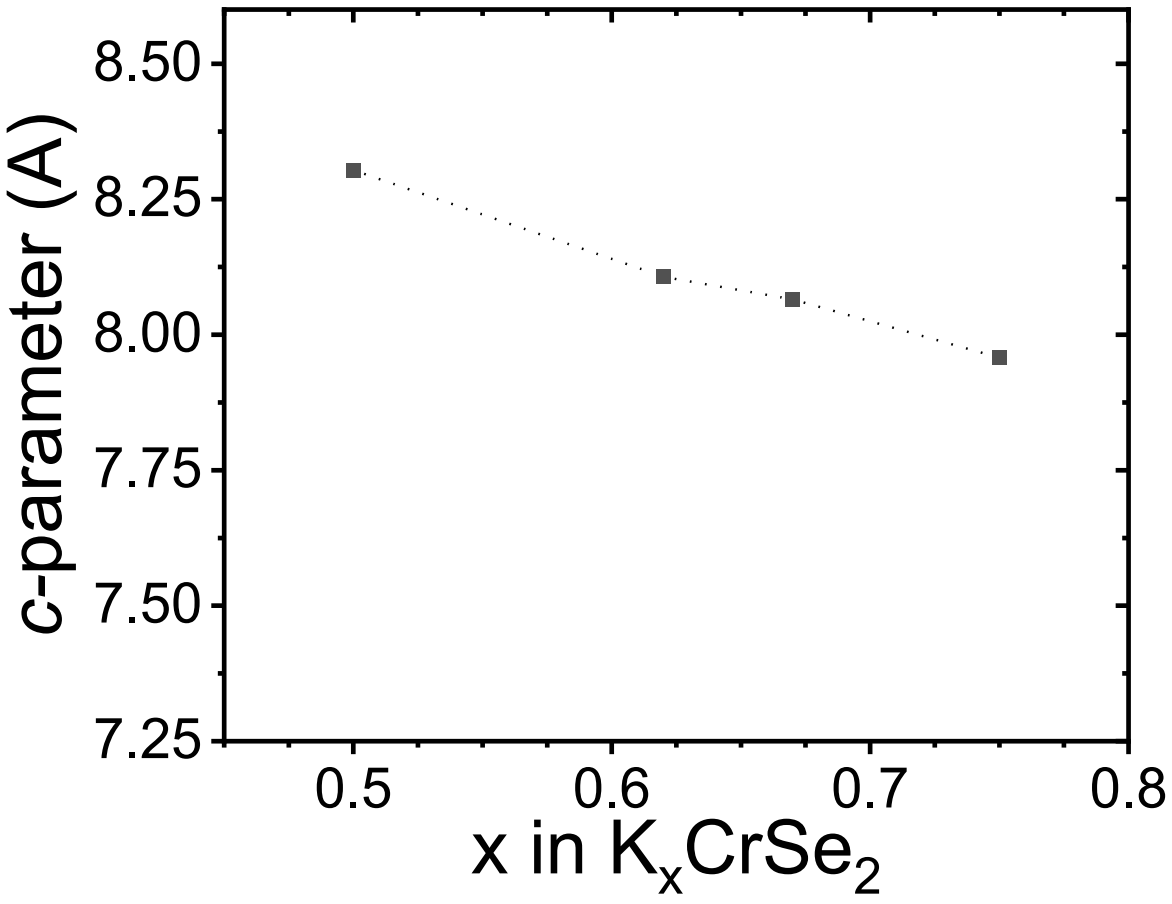

Figure S16. The *c*-parameter dependence on value of *x* within K_xCrSe_2 phases based on 009 peak of respective phases predicted by SCAN functional calculations.

Table S1. Distances (r) and disorder parameters (σ^2) obtained from the Cr K-edge EXAFS data from pristine $CrSe_2$ and $CrSe_2$ with an optimal addition of 10 wt. % of graphite. The coordination numbers (N) were fixed at the values given in *Crystallographic Information File* ICSD10313. R (fit) is a measure of the goodness of fit.

Sample	Shell	N	r, Å	σ^2, Å	R (fit)	Ref
$CrSe_2$	Cr-Se	6	2.47(1)	0.0067(2)	0.0119	This work
Graphite-added graphite	Cr-Se	6	2.47(1)	0.0069(1)	0.0076	This work
$CrSe_2$	Cr-Se	6	2.47			[28]

Table S2. Distances (r) and disorder parameters (σ^2) obtained from the Se K-edge EXAFS data from pristine from $CrSe_2$ and $CrSe_2$ with an optimal addition of 10 wt. % of graphite. The coordination numbers (N) were fixed at the values given in *Crystallographic Information File* ICSD10313. R (fit) is a measure of the goodness of fit.

Sample	Shell	N	r, Å	σ^2, Å	R (fit)
$CrSe_2$	Se-Cr	3	2.46(1)	0.0054(3)	0.0189
	Se-Se	6	3.38(1)	0.0125(10)	
	Se-Cr	3	4.19(1)	0.0173(52)	
$CrSe_2$ with an optimal addition of 10 wt. % of graphite	Se-Cr	3	2.46(1)	0.052(3)	0.0182
	Se-Se	6	3.39(1)	0.0138(11)	
	Se-Cr	3	4.19(1)	0.0175(52)	

Table S3. The summary of cell parameter of the $CrSe_2$ products determined by LeBail refinement of the experimental profile against previously reported structural model for $CrSe_2$. The standard deviations are given in parentheses.

	a, Å	*c*, Å	*V*, Å^3
$CrSe_2$ (This work)	3.3886(3)	5.9172(3)	58.844(7)
$CrSe_2$[29]	3.3898(3)	5.9099(4)	58.812(9)
$CrSe_2$@Graphite[29]	3.3910(3)	5.9144(3)	58.899(8)
$CrSe_2$[30]	3.399	5.915	59.18
$CrSe_2$[7]	3.3908	5.9099	58.846

Table S4. Electrochemical performance of layered material cathodes in nonaqueous K-Ion batteries

Cathode	Capacity mAh/g	theoretical capacity mAh/g	The number of reversible K+	Cycling life	Rate performance	Ref.
$K_{0.67}Mn_{0.95}Co_{0.05}O_2$	81 (20 mA/g)	236.51	0.36	70% (500 cycles)		[31]
$KCrS_2$	71 (0.05C)	172.67	0.41	85% (300 cycles)	39% (at 0.05C/at 5C)	[32]
$K_{0.41}CoO_2$	60 (11 mA/g)	250.49	0.23	90% (30 cycles)		[33]
$K_{0.69}CrO_2$	85 (1C)	241.55	0.47	65% (1000 cycles)	65% (at 0.1C / at 10C)	[34]
$CrSe_2$	124.98 (0.1C, 12.8 mA/g) 100.00 (1C, 128 mA/g)	127.7	1	80% (70 cycles)	85% (at 0.1 C / at 1 C)	This work

Table S5. DFT Benchmark on the structural parameters including six different functionals for $CrSe_2$ and $KCrSe_2$

	$CrSe_2$		$KCrSe_2$			
	a, Å	c, Å	a, Å	b, Å	c, Å	B, °
Experiment	3.339	5.917	6.586	3.804	7.703	106.655
PBE	3.502	5.933	6.689	3.862	7.737	106.754
PBE+D3	3.517	5.513	6.623	3.824	7.671	106.733
PBE+sol	3.440	5.590	6.570	3.794	7.608	106.735
PBEsol+D3	3.419	5.449	6.516	3.763	7.552	106.720
SCAN	3.532	5.775	6.623	3.819	7.719	106.769
SCAN + rVV10	3.523	5.698	6.608	3.812	7.684	106.797

Table S6. The unit cell parameters of K_xCrSe_2 phases

	Space group	a, Å	b, Å	c, Å	beta, °	
$KCrSe_2$	*C*2/*m*	6.5859(6)	3.8043(2)	7.7032(1)	106.655(2)	This work
$KCrSe_2$	*C*2/*m*	6.5845(2)	3.80120(10)	7.7116(2)	106.5480(10)	[7]
$K_{0.8}CrSe_2$	*C*2/*m*	6.5757(6)	3.8095(3)	7.7258(6)	106.545(11)	
$K_{0.7}CrSe_2$	*C*2/*m*	6.0965(9)	3.5043(5)	9.6532(9)	114.656(12)	
$K_{0.7}CrSe_2$	*C*2/*m*	5.9951(25)	3.5475(15)	9.6086(42)	116.000(40	
$K_{0.6}CrSe_2$	*C*2/*m*	6.3104(19)	3.7533(12)	8.2513(26)	112.384(35)	
$K_{0.6}CrSe_2$	*C*2/*m*	6.0337(8)	3.4852(4)	9.8465(6)	114.432(7)	
$K_{0.5}CrSe_2$	*C*2/*m*	6.0158(18)	3.4866(9)	9.8875(12)	114.409(16)	

References

1. M. Hamada, R. Tatara, K. Kubota, S. Kumakura and S. Komaba, *ACS Energy Letters*, 2022, **7**, 2244-2246.
2. B. H. Toby and R. B. Von Dreele, *Journal of Applied Crystallography*, 2013, **46**, 544-549.
3. X. Xue, J. Asenbauer, T. Eisenmann, G. O. Lepore, F. d'Acapito, S. Xing, J. Tübke, A. Mullaliu, Y. Li, D. Geiger, J. Biskupek, U. Kaiser, D. Steinle, A. Birrozzi and D. Bresser, *Small Structures*, 2024, **5**, 2300545.
4. B. Ravel and M. Newville, *Journal of Synchrotron Radiation*, 2005, **12**, 537-541.
5. X. H. Rui, N. Ding, J. Liu, C. Li and C. H. Chen, *Electrochimica Acta*, 2010, **55**, 2384-2390.
6. N. Elgrishi, K. J. Rountree, B. D. McCarthy, E. S. Rountree, T. T. Eisenhart and J. L. Dempsey, *Journal of Chemical Education*, 2018, **95**, 197-206.
7. X. Song, S. N. Schneider, G. Cheng, J. F. Khoury, M. Jovanovic, N. Yao and L. M. Schoop, *Chemistry of Materials*, 2021, **33**, 8070-8078.
8. J. P. Perdew, K. Burke and M. Ernzerhof, *Physical Review Letters*, 1996, **77**, 3865-3868.
9. J. P. Perdew, A. Ruzsinszky, G. I. Csonka, O. A. Vydrov, G. E. Scuseria, L. A. Constantin, X. Zhou and K. Burke, *Physical Review Letters*, 2008, **100**, 136406.
10. J. Sun, A. Ruzsinszky and J. P. Perdew, *Physical Review Letters*, 2015, **115**, 036402.
11. S. Grimme, J. Antony, S. Ehrlich and H. Krieg, *The Journal of Chemical Physics*, 2010, **132**.
12. R. Sabatini, T. Gorni and S. de Gironcoli, *Physical Review B*, 2013, **87**, 041108.
13. H. Peng, Z.-H. Yang, J. P. Perdew and J. Sun, *Physical Review X*, 2016, **6**, 041005.
14. S. Daubner, M. Dillenz, L. F. Pfeiffer, C. Gauckler, M. Rosin, N. Burgard, J. Martin, P. Axmann, M. Sotoudeh, A. Groß, D. Schneider and B. Nestler, *npj Computational Materials*, 2024, **10**, 75.
15. A. V. Krukau, O. A. Vydrov, A. F. Izmaylov and G. E. Scuseria, *The Journal of Chemical Physics*, 2006, **125**.
16. P. E. Blöchl, *Physical Review B*, 1994, **50**, 17953-17979.
17. G. Kresse and J. Hafner, *Physical Review B*, 1993, **47**, 558-561.
18. G. Kresse and J. Furthmüller, *Physical Review B*, 1996, **54**, 11169-11186.
19. G. Kresse and D. Joubert, *Physical Review B*, 1999, **59**, 1758-1775.
20. A. Van der Ven, M. K. Aydinol, G. Ceder, G. Kresse and J. Hafner, *Physical Review B*, 1998, **58**, 2975-2987.
21. M. E. Arroyo y de Dompablo, A. Van der Ven and G. Ceder, *Physical Review B*, 2002, **66**, 064112.
22. N. T. T. Tran, C.-a. Lin and S.-k. Lin, *ACS Sustainable Chemistry & Engineering*, 2023, **11**, 6978-6987.
23. H. Euchner and A. Groß, *Physical Review Materials*, 2022, **6**, 040302.
24. A. Urban, D.-H. Seo and G. Ceder, *npj Computational Materials*, 2016, **2**, 16002.
25. C. J. Bartel, *Journal of Materials Science*, 2022, **57**, 10475-10498.
26. W. Sun, S. T. Dacek, S. P. Ong, G. Hautier, A. Jain, W. D. Richards, A. C. Gamst, K. A. Persson and G. Ceder, *Science Advances*, 2016, **2**, e1600225.
27. Y. Zhang, D. A. Kitchaev, J. Yang, T. Chen, S. T. Dacek, R. A. Sarmiento-Pérez, M. A. L. Marques, H. Peng, G. Ceder, J. P. Perdew and J. Sun, *npj Computational Materials*, 2018, **4**, 9.
28. S. Kobayashi, N. Katayama, T. Manjo, H. Ueda, C. Michioka, J. Sugiyama, Y. Sassa, O. K. Forslund, M. Månsson, K. Yoshimura and H. Sawa, *Inorganic Chemistry*, 2019, **58**, 14304-14315.
29. W. Li, N. Wolff, A. Kumar Samuel, Y. Wang, V. P. Georgiev, L. Kienle and A. Y. Ganin, *ChemElectroChem*, 2023, **10**, e202300428.

30. C. F. van Bruggen, R. J. Haange, G. A. Wiegers and D. K. G. de Boer, *Physica B+C*, 1980, **99**, 166-172.
31. N. P. N. Puneeth, S. D. Kaushik and R. Kalai Selvan, *ACS Applied Energy Materials*, 2024, **7**, 2600-2613.
32. N. Naveen, W. B. Park, S. P. Singh, S. C. Han, D. Ahn, K.-S. Sohn and M. Pyo, *Small*, 2018, **14**, 1803495.
33. Y. Hironaka, K. Kubota and S. Komaba, *Chemical Communications*, 2017, **53**, 3693-3696.
34. J.-Y. Hwang, J. Kim, T.-Y. Yu, S.-T. Myung and Y.-K. Sun, *Energy & Environmental Science*, 2018, **11**, 2821-2827.